

Local structure of NiAl compounds investigated by extended X-ray absorption fine-structure spectroscopy

J. S. Tian,^{a,b} G. M. Han,^a H. Wei,^{a,c,*} T. Jin^a and M. S. Dargusch^c

^aSuperalloys Division, Institute of Metal Research, CAS, 72 Wenhua Road, Shenyang 110016, People's Republic of China, ^bGraduate School of Chinese Academy of Sciences, Beijing 100039, People's Republic of China, and ^cCAST, CRC, School of Mechanical and Mining Engineering, The University of Queensland, QLD 4072, Australia. E-mail: hwei@imr.ac.cn

The local structures of pure NiAl and Ti-, Co-doped NiAl compounds have been obtained utilizing extended X-ray absorption fine-structure (EXAFS) spectroscopy. The results provide experimental evidence that Ni antisite defects exist in the Ni-rich NiAl compounds. The site preference of Ti and Co has been confirmed. Ti occupies the Al sublattice, while Co occupies the Ni sublattice. The structure parameters obtained by EXAFS were consistent with the X-ray diffraction results. Owing to the precipitation of α -Cr, the local structure of NiAl-Cr has not been obtained, making the site preference of Cr unclear.

© 2012 International Union of Crystallography
Printed in Singapore – all rights reserved

Keywords: NiAl compounds; EXAFS; local structure; site preference; α -Cr precipitation.

1. Introduction

The NiAl compound, because of its superior high-temperature properties such as high melting point, relatively low density and good oxidation resistance, has been regarded as a potential material for use in aeroengines (Miracle, 1993). The disadvantages which limit its applications are its poor ductility and room-temperature fracture toughness (Bowman *et al.*, 1992; Noebe *et al.*, 1992). Alloying additions so far appear to be an attractive method for imparting ductility to NiAl alloy by modifying its local structure (Field *et al.*, 1991; Wei *et al.*, 2010; Zhu *et al.*, 2009). Because of the B2 structure of NiAl, the addition of alloying elements usually exhibits certain site preferences. Knowledge of the site occupancy behaviour of these alloying elements in β -NiAl is thus useful in elucidating their roles in controlling the mechanical properties.

Using first-principles calculations, Song *et al.* (2001) reported that Ti occupied the Al sublattice, Co occupied the Ni sublattice, while Cr did not show a significant preference for any sublattice. Jiang (2007) also utilized first-principles calculations when considering the effect of composition and temperature, showing that at all alloy compositions and temperatures Co had a consistent preference for the Ni sublattice, while Ti had a consistent preference for the Al sublattice. In contrast, the site preference of Cr was found to depend on both composition and temperature. Calculating the formation and site preference energies based on density function theory, Parlinski *et al.* (2003) determined that the Co and Cr atoms preferred to reside in the Ni sublattice. Fischer *et al.* (2003), using atom probe field ion microscopy, presented an alternative view that Cr had a site preference for the Al sublattice.

Despite so many results using different methods, it remains unclear as to which site the alloying elements will substitute owing to the controversy presented in the above-mentioned studies. So it is important that a solid investigation into the local structure of the NiAl compound is undertaken. With the advent of modern bright synchrotron radiation sources, the EXAFS spectroscopy technique has become a powerful tool for local structure determination, which can be applied to any type of material, *viz.* amorphous, polycrystalline, polymers, surfaces and solutions (Wang *et al.*, 2010; Wikfeldt *et al.*, 2010). Taking this into consideration, in this study EXAFS has been employed in order to investigate the local structure of pure NiAl and Ti-, Cr-, Co-doped Al-rich NiAl compounds.

2. Experiments

Elemental materials of Ni (99.95 wt% purity), Ti (99.95 wt% purity), Cr (99.95 wt% purity), Co (99.95 wt% purity) and Al (99.99 wt% purity) were first used to produce ingots of NiAl, NiAl-Ti, NiAl-Cr and NiAl-Co by vacuum induction melting. A smaller sample was then cut from the parent ingot and given a homogenization anneal at 1523 K for 100 h in a vacuum furnace at 10^{-2} Pa, followed by slow cooling to room temperature. The X-ray diffraction (XRD) patterns of the heat-treated samples exhibited sharp peaks characteristic of the B2-phase structure with no extraneous peaks. The space group is $Pm\bar{3}m$ ($Z = 1$) and the lattice constants were calculated by averaging the values derived from the three strongest peaks. All of them are listed in the corresponding Table 3 so that a comparison can be made between the EXAFS and XRD results. The chemical compositions of NiAl and NiAl-Ti,

NiAl-Cr, NiAl-Co were $\text{Al}_{48.25}\text{Ni}_{51.75}$ and $\text{Al}_{47.46}\text{Ni}_{43.63}\text{Ti}_{8.91}$, $\text{Al}_{47.79}\text{Ni}_{43.94}\text{Cr}_{8.27}$, $\text{Al}_{48.27}\text{Ni}_{44.37}\text{Co}_{7.36}$ (at%), respectively. Fine powders for EXAFS were made by crushing the annealed samples with a hardened steel mortar and pestle to a mesh size of ~ 400 .

The Ni *K*-edge EXAFS spectra of pure Ni and pure NiAl compound were collected in transmission mode because of its relatively high concentration, which was higher than 10 at%. However, to obtain the neighbouring environment of the alloying elements, *K*-edge EXAFS spectra of the alloying elements, namely Ti, Cr, Co, were collected in fluorescence mode owing to their low concentration (<10 at%). All of the experiments were performed at the 1W1B beamline of the Beijing Synchrotron Radiation Facility at room temperature. For this study the electron-beam energy was 2.2 GeV with a stored current between 150 mA and 250 mA. The synchrotron radiation emitted by the storage ring was monochromated by a double-crystal Si (111) monochromator and focused on the sample. The energy resolution $\Delta E/E$ is smaller than 3×10^{-4} at 9 keV. To eliminate machine error, before the collection the energy was calibrated using the corresponding pure metal foil. The EXAFS collection was divided into five steps; for every step the energy step and acquisition time were different (Table 1). An ion chamber and Lytle detector were used for the transmission mode and fluorescence mode, respectively.

There is something important to take into account for the EXAFS collection. For the transmission mode, the thickness effect is a key factor that will reduce the EXAFS amplitudes. To minimize the thickness effect, the samples were ground and sifted through a 400 mesh, and then the powders were spread onto 3M adhesive tape. By controlling the layer number of the tape, an absorption length of $\mu t \simeq 1$ was obtained. For the fluorescence mode, the self-absorption (SA) effect affects the EXAFS amplitudes. The samples were sufficiently thin that the SA effect could be neglected. This was also confirmed when the SA module of the *Athena* software was used.

All EXAFS data were fitted using *IFEFFIT* (Newville, 2001) to *ab initio* theoretical standards generated by *FEFF* (Rehr *et al.*, 1991). The *FEFF* file was built using data of stoichiometric composition at room temperature whose lattice constant was 2.8870 Å (Taylor & Doyle, 1972).

3. Results and discussions

Fig. 1(a) shows the k^3 -weighted $\chi(k)$ of the Ni *K*-edge EXAFS spectrum following a standard procedure of pre-edge and post-edge background removal, step normalization at the edge, extraction of the XAFS signal $\chi(k)$, and k^3 weighting to highlight the region at high k . A Fourier transformation was performed to transfer the k space to R space so that the radial structural function (RSF) was obtained [Fig. 1(b), black line]. The first peak at about 2.0 Å in the Fourier transform (FT) of the Ni *K*-edge EXAFS spectrum corresponds to the contribution from the first shell around the Ni absorber (Ni–Al), and the second peak at about 2.6 Å corresponds to the second shell (Ni–Ni). We have to underline the fact that the positions of the peaks in the FT are shifted by a few tenths of an

Table 1
Data collection information.

E_0 is the absorption-edge energy. Different regions have different energy steps and scan times. The scan time of the transmission mode is listed, with that of the fluorescence mode in parentheses.

Region	Start energy (eV)	End energy (eV)	Energy step (eV)	Scan time (s)
Pre-edge	$E_0 - 200$	$E_0 - 20$	4	1 (5)
XANES	$E_0 - 20$	$E_0 + 30$	0.7	1 (5)
EXAFS1	$E_0 + 30$	$E_0 + 200$	2	2 (5)
EXAFS2	$E_0 + 200$	$E_0 + 800$	3	3 (5)
EXAFS3	$E_0 + 800$	$E_0 + 1000$	4	3 (5)

angstrom from the actual interatomic distances because of the EXAFS phase shift (Rehr & Albers, 2000). An inverse FT [Fig. 1(b) (inset), black line] was performed to isolate the EXAFS contribution from a selected region with a sine window in R space.

To obtain a quantitative result, both the first shell and the second shell of the EXAFS spectrum were fitted in the range $2\text{--}14 \text{ \AA}^{-1}$ in k space and $1.2\text{--}2.8 \text{ \AA}$ in R space due to the fact that the FT has a sharp cusp between the first and second peak which is often an indication of strong interference from two or more components in the EXAFS. To make sure that all the

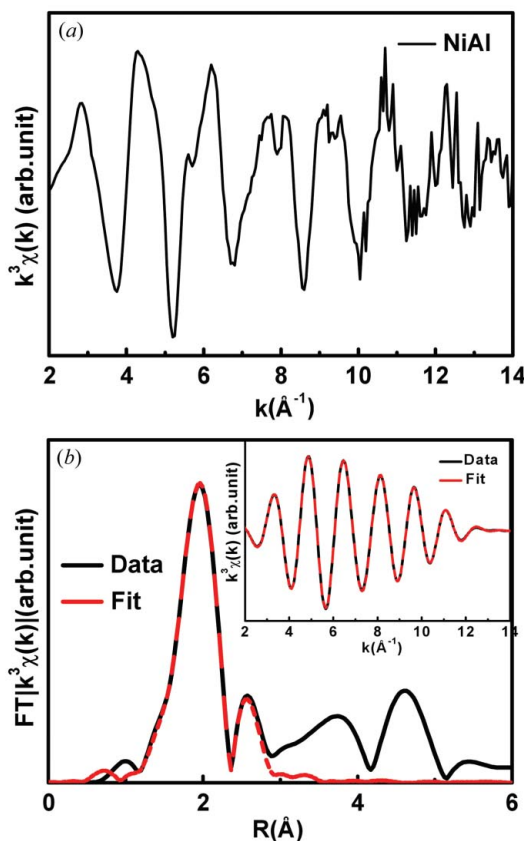


Figure 1
(a) k^3 -weighted $\chi(k)$ of the Ni *K*-edge EXAFS spectrum for pure NiAl and (b) fit for the Ni *K*-edge EXAFS spectrum of pure NiAl in R space and k space (inset) in the range $2\text{--}14 \text{ \AA}^{-1}$ in k space and $1.2\text{--}2.8 \text{ \AA}$ in R space. The superposition between the experimental curve and the fitted curve indicates a good fit.

corresponding paths were considered, another path of the higher shell was also checked, and was found to have a negligible contribution to the first and second shell. The number of independent parameters which can be determined by EXAFS is limited by the number of independent data points $N_{\text{ind}} \simeq (2\Delta k \Delta R)/\pi$, where Δk and ΔR are the ranges of the fit in the k and R space, respectively. In this case, Δk was about 12 \AA^{-1} and ΔR was about 1.6 \AA ,

so $N_{\text{ind}} \simeq 12$, which is adequate for obtaining the required parameters for the pure NiAl compound. During fitting, the amplitude reduction factor (S_0^2) was fixed to 0.83, obtained by fitting the EXAFS of pure Ni owing to the fact that S_0^2 is insensitive to the chemical environment while depending on the type of absorber, whilst the energy shift ΔE_0 was considered to be the same value for Ni–Al and Ni–Ni. The coordination number of Ni–Ni and that of Ni–Al could be altered during fitting, whilst the Debye–Waller factor σ^2 was considered to be different for Ni–Ni and Ni–Al, since the masses of the two atoms are different and may affect the thermal vibrations.

Fig. 1(b) shows the experimental curve and fitted curve of the EXAFS spectrum both in k space and in R space; the black full line represents the experimental curve and the grey dashed line (red online) represents the fitted curve. One can distinctly see that the experimental curve and the fitted curve superpose almost over the whole range, indicating that the result was satisfactory. The structure parameters are listed in Table 2, in which the R -factor is a standard function used to evaluate the quality of the fit. Generally, a small R -factor (<2%) is required for a good fit. It can be seen that the R -factor for our fit is much smaller than 2%. This suggests that we have obtained a satisfactory fit. Other parameters have been interpreted as follows: N is the coordination number and R is the mean distance between the absorbing atom and its neighbours, σ^2 is the mean-square deviation from R owing to the static disorder and thermal motivation and ΔE_0 is the energy shift compared with the standard sample. Table 2 shows that not only Al atoms but also Ni atoms are coordinating with the absorbing Ni atom, namely that superfluous Ni atoms substitute for Al atoms, forming Ni antisite defects in the Ni-rich NiAl compound. This result is consistent with the BT model proposed by Bradley & Taylor (1937) which has been confirmed by XRD and density measurements.

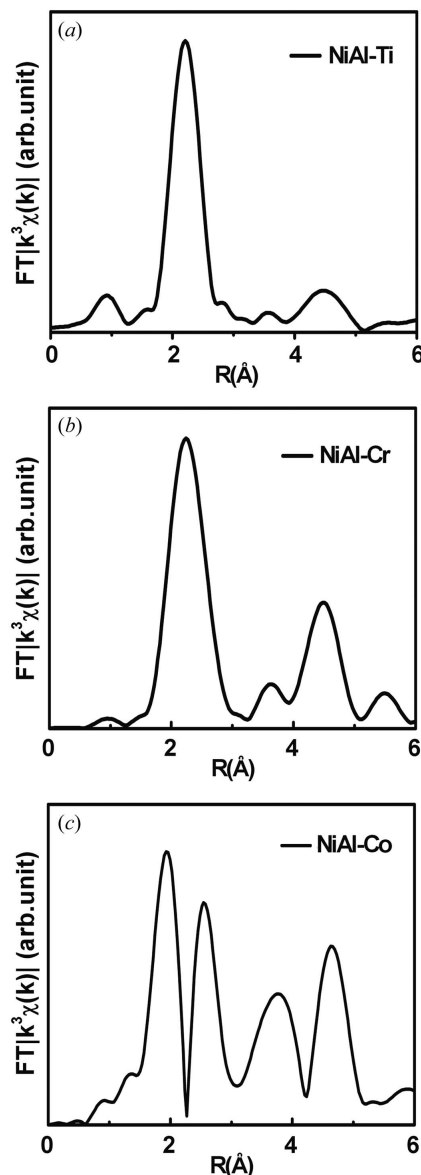
The same procedure was then applied to the EXAFS spectra of the Ti-, Cr- and Co-doped NiAl compounds. The FTs of the EXAFS spectra are presented in Fig. 2. According to the figure, it can be seen that the radial structural functions (RSFs) of NiAl-Ti and NiAl-Cr are quite different from the RSF of NiAl-Co. For NiAl-Co the k^3 -weighted FT of the EXAFS function exhibits an almost resolved doublet, while for NiAl-Ti and NiAl-Cr it is no longer a doublet. Chartier *et al.* (1994) and Balasubramanian *et al.* (1995) also reported these phenomena when they studied Fe- or Co-doped NiAl

Table 2

Structure parameters obtained by fitting the Ni K -edge EXAFS spectrum of pure NiAl.

N is the coordination number, R is the mean distance between the absorbing atom and its neighbours, σ^2 is the mean-square deviation from R owing to the static disorder and thermal motivation, ΔE_0 is the energy shift compared with the standard sample, and R -factor is a standard function used to evaluate the quality of the fit. A small R -factor suggests a good fit. 0.2 Ni atoms substitute for the Al atoms forming Ni antisite defects. This is consistent with the BT model.

Sample	Shell	Bond type	N	R (\AA)	σ^2 (10^{-3} \AA^2)	ΔE_0	R -factor
NiAl	First	Ni–Al	7.8 ± 0.75	2.44 ± 0.04	12 ± 4	3.0 ± 1.8	0.002
		Ni–Ni	0.2 ± 0.02	2.43 ± 0.03	15 ± 6	3.0 ± 1.8	
	Second	Ni–Ni	6 ± 0.58	2.83 ± 0.04	15 ± 6	3.0 ± 1.8	

**Figure 2**

k^3 -weighted FT of (a) the Ti K -edge for NiAl-Ti, (b) the Cr K -edge for NiAl-Cr and (c) the Co K -edge for NiAl-Co. The radial structural functions (RSFs) of NiAl-Ti and NiAl-Cr are quite different from the RSF of NiAl-Co. For NiAl-Co the k^3 -weighted FT of the EXAFS function exhibits an almost resolved doublet, while for NiAl-Ti and NiAl-Cr it is no longer a doublet. This indicates that they have a different site preference. Based on the hypothesis by Chartier *et al.* (1994) and Balasubramanian *et al.* (1995), it can be concluded that Ti and Cr prefer to reside in the Al site while Co prefers to reside in the Ni site.

Table 3

Structure parameters obtained by fitting Ti *K*-edge EXAFS and Co *K*-edge EXAFS.

The parameters have the same meaning as those in Table 2. It is clear that Ti occupies the Al sublattice while Co occupies the Ni sublattice. The parameters obtained from XRD are also given for comparison with the EXAFS results. It can be seen that they are consistent.

Sample	Shell	Bond type	<i>N</i>	<i>R</i> (Å)	<i>R</i> (XRD) (Å)	σ^2 (10^{-3} Å ²)	ΔE_0	<i>R</i> -factor (10^{-3})
NiAl-Ti	First	Ti–Ni	7.9 ± 0.8	2.52 ± 0.01	2.5140	3.8 ± 0.09	6.3 ± 1.7	1.0
	Second	Ti–Al	6 ± 0.6	2.88 ± 0.03	2.9029	5.9 ± 3.2	6.3 ± 1.7	
NiAl-Co	First	Co–Al	8 ± 0.3	2.46 ± 0.06	2.4819	7.4 ± 2.2	4.1 ± 1.2	3.2
	Second	Co–Ni	5.8 ± 0.2	2.84 ± 0.06	2.8658	13 ± 1.9	4.1 ± 1.2	

compounds. These authors suggested that the general appearance of the FT is therefore a ‘fingerprint’ and gives a first indication of the type of site occupation in these systems, which can then be confirmed by standard fitting procedures. Based on this hypothesis, the site preference of Ti, Cr and Co has been obtained, with Co occupying the Ni sites and Ti and Cr substituting for the Al sites.

To validate this hypothesis, the fit for Co in NiAl-Co was obtained using a two-shell fit assuming that the Co atoms occupied the Ni sublattice, while the fit for NiAl-Ti was obtained by a two-shell fit assuming that the Ti atoms occupied the Al sublattice. The fits were performed both in *R* space and in *k* space, as shown in Fig. 3, and the structure parameters have been provided in Table 3. For NiAl-Ti the *R* range and *k* range is about 3.6–12.7 Å⁻¹ and 1.3–3.0 Å, respectively, while for NiAl-Co the value is about 2.3–12.4 Å⁻¹ and 1.1–3.0 Å, respectively. *S*₀² for Ti and Co was fixed to 0.86 (3) (Arçon *et al.*, 2001) and 0.79, respectively. Other parameters were set using the same principle as with the Ni-edge fitting. There is a good agreement between the experimental curve and the fitted curve. The structure parameters listed in Table 3 confirm the hypothesis of Chartier *et al.* (1994) and Balasubramanian *et al.* (1995).

The parameters obtained by XRD are also listed in Table 3 to make a clear comparison with the EXAFS results. It can be seen that, by using the two different methods, the lattice parameters are consistent. They are also consistent with the local density LMTO (linear muffin-tin orbital) method of Medvedeva *et al.* (1998), with the TEM/EDS technique of ALCHEMI (atom location channeling enhanced microanalysis) for Ti of Wilson & Howe (1999), with the Bozzolo–Ferrante–Smith method of Bozzolo *et al.* (2002), and with first-principles calculations of binding energy combined with the mean-field model for Co and Ti of Hao *et al.* (2003).

According to the widely invoked BT model, in the Al-rich NiAl compound the Al antisite defects caused by an excess of Al atoms are not formed, thus resulting in the creation of substantial constitutional vacancies on the Ni sites, *i.e.* the creation of Ni vacancies. This is consistent with our results.

Since there are good fits for the NiAl-Co and NiAl-Ti compounds, one may expect a good fit for NiAl-Cr too. However, this is not the case when fitting the EXAFS spectrum of NiAl-Cr; it is not possible to obtain a good fit for a wide range of parameters. This suggests that the local structure of NiAl-Cr is more complicated than that of the NiAl-Ti and NiAl-Co compounds. It is well known that Cr has a small solid solution limit of about 2 at% (Cotton *et al.*, 1993) in the NiAl

compound at room temperature, much smaller than the 8.27 at% of our NiAl-Cr sample. During cooling after homogenizing annealing, α-Cr precipitates (Field *et al.*, 1991; Villars *et al.*, 1995) also with a body-centred cubic structure whose lattice constant is 2.884 Å, comparable with the 2.887 Å of NiAl. Because of their similar structure and comparable lattice constants, the EXAFS spectrum is regarded as a combination of α-Cr and NiAl-Cr, making it impossible to fit. It is important to note that owing to the lack of a fit for NiAl-Cr the site preference of Cr in the NiAl compound cannot be confirmed.

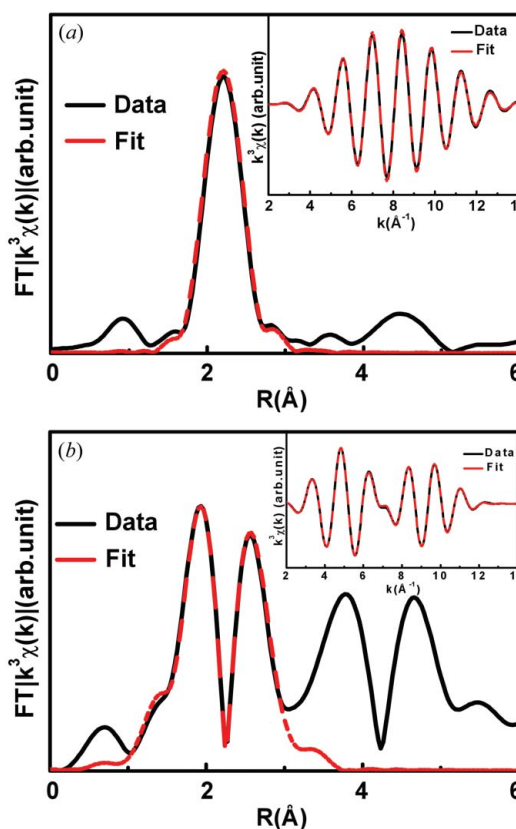


Figure 3 Fit both in *R* space and *k* space (inset) for (a) Ti *K*-edge EXAFS of NiAl-Ti assuming Ti goes exclusively to Al sites and (b) Co *K*-edge EXAFS of NiAl-Co assuming Co goes exclusively to Ni sites, based on the hypothesis by Chartier *et al.* (1994) and Balasubramanian *et al.* (1995). For NiAl-Ti the *R* range and *k* ranges are about 3.6–12.7 Å⁻¹ and 1.3–3.0 Å, respectively, while for NiAl-Co the values are about 2.3–12.4 Å⁻¹ and 1.1–3.0 Å, respectively. There is a good agreement between the experimental curve and the fitted curve. The fitting results confirm the hypothesis.

Research by Fox & Tabbernor (1991) showed that the electron distribution of pure NiAl is a depletion of electrons from the regions along $\langle 100 \rangle$ between next-nearest neighbours (NNNs) and a concomitant increase in electron density between nearest-neighbour (NN) Ni–Al atom pairs along the $\langle 111 \rangle$ direction. This results in a strong covalent bond between NN Ni–Al atom pairs and a weak ionic repulsion between the NNN atoms along the $\langle 100 \rangle$ direction, and these directional bonds are superimposed over a metallic bond. This is the reason that pure NiAl possesses a poor ductility. While alloying has been shown to improve the ductility both by experiments (Darolia *et al.*, 1992) and by first-principles calculations (Medvedeva *et al.*, 1998), the mechanism remains under debate. To have a deep understanding of the micro-mechanism in the electron point of view, the local structure must be obtained first. Based on this work the electronic structure and the relationship between the structure and the property will be discussed further by combining X-ray absorption near-edge structure (XANES), X-ray photoelectron spectra and first-principles calculations. Corresponding works are under preparation.

4. Conclusions

The EXAFS method has been employed to investigate the local structure of pure NiAl and Ti-, Cr-, Co-doped NiAl compounds. In the Ni-rich pure NiAl the presence of the Ni antisite defect has been confirmed. The structure parameters indicate unambiguously that Ti occupies the Al sublattice, while Co occupies the Ni sublattice. Owing to the complicated structure caused by the precipitation of α -Cr, the local structure of the NiAl–Cr compound and the site preference of Cr have not been obtained.

This work was supported by a grant from the Major State Basic Research Development Program (973 Program) of China under grant No. 2010CB631200 (2010CB631206) and from the National Natural Science Foundation of China (NSFC) (Nos. 50931004, 51071164 and 50671102). We would like to thank Beijing Synchrotron Radiation Facility and the National Synchrotron Radiation Laboratory, University of Science and Technology of China for EXAFS measurements and data analysis.

References

- Arçon, I., Tuel, A., Kodre, A., Martin, G. & Barbier, A. (2001). *J. Synchrotron Rad.* **8**, 575–577.
- Balasubramanian, M., Pease, D. M., Budnick, J. I., Manzur, T. & Brewé, D. L. (1995). *Phys. Rev. B*, **51**, 8102–8106.
- Bowman, R. R., Noebe, R. D., Raj, S. V. & Locci, L. E. (1992). *Metall. Trans. A*, **23**, 1493–1508.
- Bozzolo, G., Noebe, R. D. & Amador, C. (2002). *Intermetallics*, **10**, 149–159.
- Bradley, A. J. & Taylor, A. (1937). *Proc. R. Soc. London Ser. A*, **159**, 56–72.
- Chartier, P., Balasubramanian, M., Brewé, D., Manzur, T., Pease, D., Budnick, J., Huang, L., Law, C., Russel, L. & Kimball, C. (1994). *J. Appl. Phys.* **75**, 3842–3846.
- Cotton, J. D., Noede, R. D. & Kaufman, M. J. (1993). *Intermetallics*, **1**, 3–20.
- Darolia, R., Lahrman, D. & Field, R. (1992). *Scr. Metall. Mater.* **26**, 1007–1012.
- Field, R. D., Lahrman, D. F. & Darolia, R. (1991). *Acta Metall. Mater.* **39**, 2961–2969.
- Fischer, R., Frommeyer, G. & Schneider, A. (2003). *Mater. Sci. Eng. A*, **353**, 87–91.
- Fox, A. G. & Tabbernor, M. A. (1991). *Acta Metall. Mater.* **39**, 669–678.
- Hao, Y. L., Yang, R., Hu, Q. M., Li, D., Song, Y. & Niionomi, M. (2003). *Acta Mater.* **51**, 5545–5554.
- Jiang, C. (2007). *Acta Mater.* **55**, 4799–4806.
- Medvedeva, N. I., Gornostyrev, Y. N., Novikov, D. L., Mryasov, O. N. & Freeman, A. J. (1998). *Acta Mater.* **46**, 3433–3442.
- Miracle, D. B. (1993). *Acta Metall. Mater.* **41**, 649–684.
- Newville, M. (2001). *J. Synchrotron Rad.* **8**, 322–324.
- Noebe, C. L., Cullers, R. D. & Bowman, R. R. (1992). *J. Mater. Res.* **7**, 605–612.
- Parlinski, K., Jochym, P. T., Kozubski, R. & Oramus, P. (2003). *Intermetallics*, **11**, 157–160.
- Rehr, J. J. & Albers, R. C. (2000). *Rev. Mod. Phys.* **72**, 621–654.
- Rehr, J. J., Mustre de Leon, J., Zabinsky, S. I. & Albers, R. C. (1991). *Phys. Rev. B*, **44**, 4146–4156.
- Song, Y., Guo, Z. X., Yang, R. & Li, D. (2001). *Acta Mater.* **49**, 1647–1654.
- Taylor, A. & Doyle, N. J. (1972). *J. Appl. Cryst.* **5**, 201–209.
- Villars, P., Prince, A. & Okamoto, H. (1995). Editors. *Handbook of Ternary Alloy Phase Diagrams*, pp. 3152–3162. Metals Park: ASM.
- Wang, C. H., Guo, Y. Z., Casper, F., Balke, B., Fecher, G. H., Felser, C. & Hwu, Y. (2010). *Appl. Phys. Lett.* **97**, 103106.
- Wei, H., Liang, J. J., Wei, H., Sun, B. Z., Zheng, Q., Sun, X. F., Peng, P., Dargusch, M. S. & Yao, X. (2010). *Philos. Mag. Lett.* **90**, 225–230.
- Wikfeldt, K. T., Leetmaa, M., Mace, A., Nilsson, A. & Pettersson, L. G. (2010). *J. Chem. Phys.* **132**, 104513.
- Wilson, A. W. & Howe, J. M. (1999). *Scr. Mater.* **41**, 327–331.
- Zhu, J., Zhang, C., Cao, W., Yang, Y., Zhang, F., Chen, S., Morgan, D. & Chang, Y. A. (2009). *Acta Mater.* **57**, 202–212.